

RESEARCH ARTICLE

Distinct gene-selective roles for a network of core promoter factors in *Drosophila* neural stem cell identity

Alexandre Neves* and Robert N. Eisenman*

ABSTRACT

The transcriptional mechanisms that allow neural stem cells (NSC) to balance self-renewal with differentiation are not well understood. Employing an *in vivo* RNAi screen we identify here NSC-TAFs, a subset of nine TATA-binding protein associated factors (TAFs), as NSC identity genes in *Drosophila*. We found that depletion of NSC-TAFs results in decreased NSC clone size, reduced proliferation, defective cell polarity and increased hypersensitivity to cell cycle perturbation, without affecting NSC survival. Integrated gene expression and genomic binding analyses revealed that NSC-TAFs function with both TBP and TRF2, and that NSC-TAF-TBP and NSC-TAF-TRF2 shared target genes encode different subsets of transcription factors and RNA-binding proteins with established or emerging roles in NSC identity and brain development. Taken together, our results demonstrate that core promoter factors are selectively required for NSC identity *in vivo* by promoting cell cycle progression and NSC cell polarity. Because pathogenic variants in a subset of TAFs have all been linked to human neurological disorders, this work may stimulate and inform future animal models of TAF-linked neurological disorders.

KEY WORDS: TAFs, Neural stem cells, Transcription

INTRODUCTION

Brains from a wide range of animal species are populated by neural stem cells (NSCs). NSCs must balance self-renewal with differentiation, and failure to achieve this balance can lead to neurological disorders. For example, excess self-renewal of NSCs has been linked to brain tumors whereas premature depletion of NSCs is thought to contribute to primary microcephaly, a human neurological disorder characterized by markedly reduced brain size at birth (Fish et al., 2006; Lancaster et al., 2013; Lee et al., 2018). In the last decade, *Drosophila* NSCs have emerged as a powerful *in vivo* system to study NSC identity because they provide a genetically tractable model that recapitulates many important features of mammalian NSC biology including asymmetric cell division, coupling between the cell cycle and cell fate and a dependence on conserved polarity complexes (Homem and Knoblich, 2012).

Two major types of NSCs have been shown to populate the *Drosophila* central brain. Type I NSCs express two related bHLH


transcription factors, Asense (Ase) and Deadpan (Dpn), and divide asymmetrically into a single type I NSC and into a differentiating daughter, the ganglion mother cell (GMC). The GMC then undergoes a terminal division to give rise to two post-mitotic neurons. In contrast, type II NSCs express Dpn but not Ase, and divide into another type II NSC and an intermediate neuronal progenitor (INP). After maturation, the INP expresses Ase and undergoes limited rounds of self-renewing divisions while also generating GMCs, much like a type I NSC (Fig. 1A). Asymmetric distribution of cell fate determinants such as the transcription factor Prospero and the RNA-binding protein Brat is thought to control differentiation in type I and type II lineages respectively (Choksi et al., 2006; Boone and Doe, 2008; Bowman et al., 2008; Bello et al., 2008). In contrast to the many genes that have been identified to be required for NSC differentiation, the gene regulatory networks that control NSC identity are less well understood. Here we define NSC identity as the suite of stem cell attributes such as asymmetric cell division, self-renewal, survival, growth and proliferation that collectively distinguish NSCs from their differentiating and differentiated progeny.

In order to understand in more detail the basis for NSC identity we carried out a focused RNAi screen in live *Drosophila*, testing transcriptional regulators that influence the number of NSCs and the size of NSC lineages (Fig. 1B). Unexpectedly we found that a subset of TAFs (TATA box-binding protein-associated factors) and the TBP-related factor 2 (TRF2) are required for maintaining normal NSC numbers, NSC proliferation and NSC cell polarity, but do not appear to be required for NSC survival. We further found that NSCs depleted of TAFs or TRF2 are hypersensitive to cell cycle manipulation. TAFs have been well characterized as subunits of the ~1 megadalton Transcription Factor IID (TFIID) complex comprised of the TATA box-binding protein (TBP) and 13 individual TAFs (Fig. 1C) (Goodrich and Tjian, 2010). The main function of TFIID is to recognize and bind to the core promoter, a segment of DNA that is sufficient to direct accurate and efficient RNA polymerase II transcription.

A number of recent studies suggest that some TFIID subunits are neither universally required for gene expression nor invariant (Zhou et al., 2013; Hiller et al., 2004; Goodrich and Tjian, 2010). However, while different subsets of TFIID subunits have been shown to be required for the self-renewal of both murine and human embryonic stem cells (ESCs), the function of TAFs in stem cell populations *in vivo* has not been investigated (Pijnappel et al., 2013; Maston et al., 2012). Notably, a number of recent genetic studies have identified pathogenic variants in several TFIID subunits. First, variants in *TAF1*, *TAF2*, *TAF8* and *TAF13* have all been linked to intellectual disability and microcephaly (O'Rawe et al., 2015; Hellman-Aharony et al., 2013; Tawamie et al., 2017; El-Saafin et al., 2018). Second, insertion of an SVA-type retrotransposon in a noncoding region of *TAF1*, that results in abnormal splicing and reduced expression of *TAF1* in patient-derived NSCs, is associated

Basic Sciences Division, Fred Hutchinson Cancer Research Center, Seattle, WA 98109-1024, USA.

*Authors for correspondence (aneves@fredhutch.org; eisenman@fredhutch.org)

 A.N., 0000-0003-2775-8447; R.N.E., 0000-0002-0274-9846

This is an Open Access article distributed under the terms of the Creative Commons Attribution License (<https://creativecommons.org/licenses/by/4.0>), which permits unrestricted use, distribution and reproduction in any medium provided that the original work is properly attributed.

Received 31 January 2019; Accepted 20 February 2019

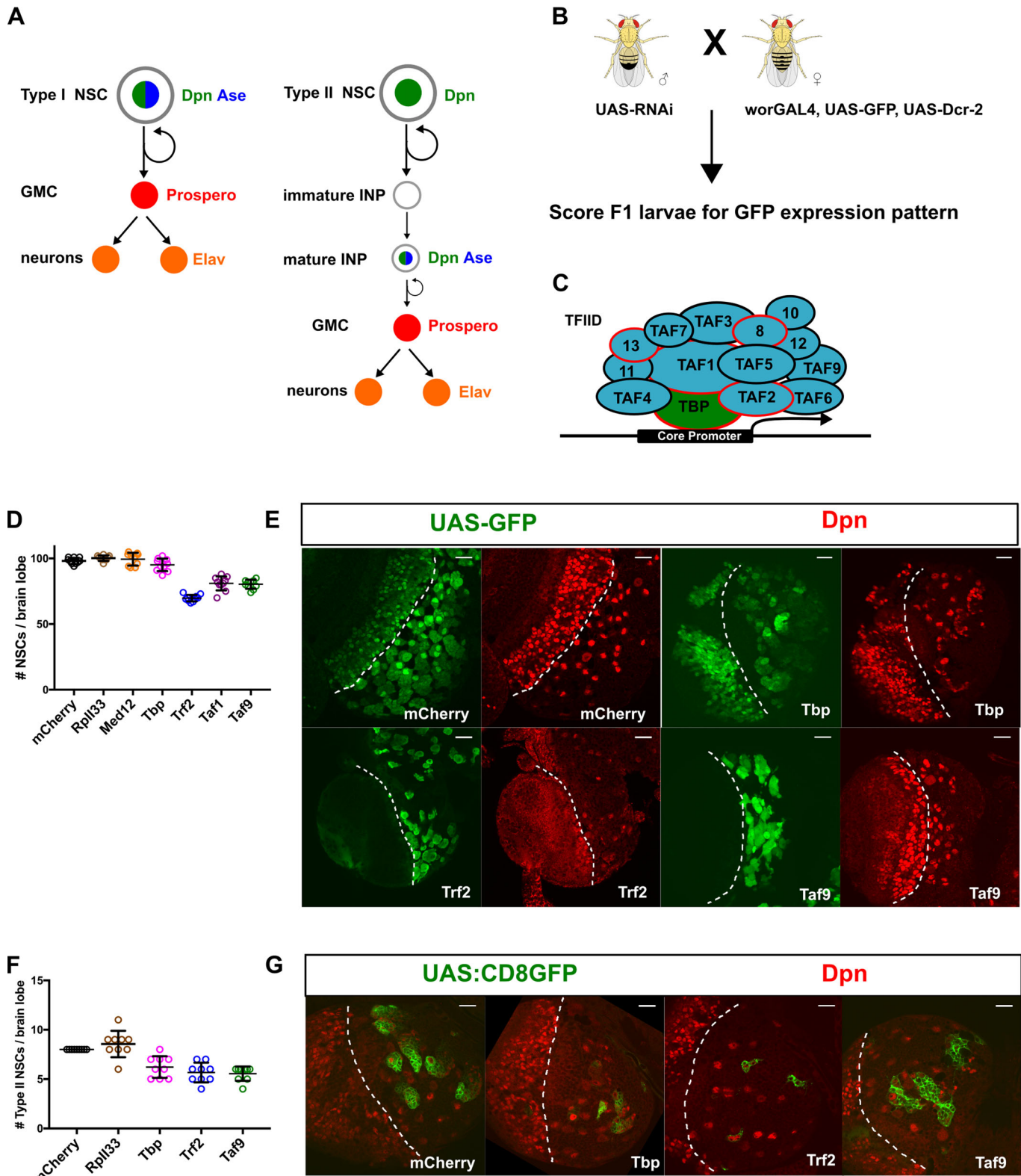


Fig. 1. See next page for legend.

with X-linked dystonia parkinsonism (Bragg et al., 2017; Aneichyk et al., 2018). Third, *TBP* is a candidate microcephaly and intellectual disability gene in patients with a subtelomeric 6q deletion, whereas *de novo* expansion of CAG repeats in *TBP* is thought to cause spinocerebellar ataxia 17 (Rooms et al., 2006; Hsu

et al., 2014). Finally, mutations in *TAF6* have been linked to a Cornelia de Lange-like syndrome, a clinically heterogeneous disorder characterized by developmental delay and intellectual disability (Yuan et al., 2015). In this study, we extend the role of TAFs, TBP and TRF2 in developmental gene regulation by showing

Fig. 1. A unique subset of TAFs (NSC-TAFs) required for NSC

homeostasis. (A) Marker gene expression and cell division patterns of Type I (left) and Type II (right) NSCs. (B) Genetic schema of *in vivo* transgenic RNAi screen. (C) Subunit composition of Transcription Factor IID (TFIID); the red outline indicates subunits implicated in human neurological disorders. (D) Quantification of total central brain NSCs (large Dpn⁺ cells) in nervous systems expressing the listed RNAi transgenes using a pan-NSC driver (worniuGAL4, UAS-Dcr-2, UAS-GFP). *P*-values were RpII33 (0.6655), MED12 (0.9376), TBP (0.3182), TRF2 (<0.001), TAF1 (<0.001), TAF9 (<0.001). (E) Single confocal section of brain lobes expressing the indicated RNAi transgenes showing expression of either UAS-GFP (left) or the NSC marker Dpn (right). (F) Quantification of Type II NSCs in nervous systems expressing the listed transgenes using a Type II NSC driver (UAS-Dcr-2; worniuGAL4, aseGAL80, UAS-CD8:GFP). CD8:GFP is a membrane targeted GFP transgene. *P*-values were RpII33 (0.5449), TBP (0.0011), TRF2 (<0.0001), TAF9 (<0.0001). (G) Single confocal section of brain lobes expressing the listed RNAi transgenes showing expression of either UAS-CD8:GFP (left) or the NSC marker Dpn (right). In D and F, experimental genotypes were compared to the mCherry control using a one-way ANOVA with Dunnett's multiple comparison test. In E and G, the white dotted line demarcates the optic lobe (left)/central brain (right) boundary. Scale bars: 20 μ m. Note that TRF2 or TAF9 depletion leads to increased GFP expression in the central brain whereas TBP depletion leads to decreased GFP expression; compare with optic lobe GFP expression.

they are members of a core promoter network involved in NSC identity.

RESULTS

A subset of TAFs is required for NSC identity

To identify genes that regulate NSC identity, we performed a focused transgenic *in vivo* RNAi screen using an NSC-enriched GAL4 driver line (worniu-GAL4, UAS-GFP, UAS-Dcr-2) to drive expression of either long or short hairpin RNAs (Fig. 1B). We used the intensity and pattern of the GFP signal in live wandering larvae as a proxy for NSC identity. After testing more than 900 RNAi transgenes, we focus here on the functional analysis of hits targeting genes encoding TAFs. We found that knockdown of any one of nine different TAFs (*Taf1*, *Taf2*, *Taf4*, *Taf5*, *Taf6*, *Taf7*, *Taf8*, *e(y)1/Taf9*, *Taf12*) resulted in a complex suite of similar phenotypes: fewer NSCs, with remaining NSCs clustering together, smaller NSC lineages, abnormal morphology, reduced expression of the type I NSC marker *Ase* whereas expression of the pan-NSC marker *Dpn* remained unaffected (Fig. 1D,E, see Fig. 2D,F,H for *Ase* expression). While the observed NSC loss was moderate, it was highly reproducible and comparable to that observed upon either knockdown or loss of function of other NSC identity genes (Zhu et al., 2012; Lai et al., 2012; Rust et al., 2018). To test whether increased levels of NSC-TAFs can promote NSC fate, we overexpressed a number of different NSC-TAFs as well as additional core promoter factors but did not observe any overt phenotypes (Fig. S1A,B). As a positive control, we overexpressed a constitutively active form of aPKC (Lee et al., 2006), a known NSC identity gene and observed the expected increase in brain size. Intriguingly, knockdown of other prototypical TAFs (*bip2/Taf3*, *Taf10*, *Taf10b*, *Taf11*, *Taf13*) did not result in overt phenotypes (Fig. S2A,B, Table S1). The lack of an observable NSC phenotype for these TAFs is unlikely to be due to inefficient RNAi since knockdown of either *Taf3* or *Taf13* with actin-GAL4 resulted in highly penetrant organismal lethality, findings that are consistent with an independent genome-wide RNAi screen (Neumüller et al., 2011). Moreover, NSC clones that were homozygous for lethal alleles of *Taf11* (*Taf11^{MI}* and *Taf11^{M5}*; Liang et al., 2015) or *Taf13* (*Taf13^{LL04552}*; Schuldiner et al., 2008), generated using the MARCM (Mosaic Analysis with a Repressible Cell Marker) (Lee

and Luo, 1999) system, were either modestly reduced in size (*Taf11^{MI}* and *Taf11^{M5}*) or indistinguishable (*Taf13^{LL04552}*) from their wild-type counterparts both in terms of NSC clone size and *Ase* expression (Fig. S2A,C).

TBP, TRF2 and TAF depletion results in shared and private phenotypes

For clarity, we refer to the subset of TAFs that presented a phenotype in our screen as NSC-TAFs. *Drosophila* TAFs are known to be present in either Transcription Factor IID (Fig. 1C, TFIID, composed of TBP and 13 TAFs) or SAGA (Spt-Ada-Gcn5-acetyltransferase; including TAF9, TAF10b, TAF12). However, knocking down TBP or SAGA-specific subunits (*Gcn5*, *Spt3*, *Saf6*, *Spt7*) did not cause a reduction in NSC numbers, or affect *Ase* expression, despite a marked reduction in the both the GFP signal and organismal viability (Fig. 1D; Table S1). Moreover, reducing expression of other components of the transcription initiation complex by knocking down subunits of RNA Polymerase II (RpII33) or the Mediator (MED12) complex, reduced the size of NSC lineages without decreasing NSC numbers (Fig. 1D). These data suggest that gene-selective functions of TAFs, rather than general transcriptional activity, are required for NSC identity.

Metazoan lineages evolved several paralogs of TBP called TBP-related factors (TRFs), with TRF1 and TRF3 only found in insect and vertebrate clades, respectively, whereas TRF2 is conserved in all bilaterians (Duttke et al., 2014). We were intrigued that TBP knockdown and NSC-TAF knockdown phenotypes were different, since TAFs and TBP are thought to be obligate partners. We hypothesized that in addition to functioning with TBP as part of TFIID, TAFs may also function with a TBP paralog. Based on previous studies (Takada et al., 2000; Fan et al., 2017; Kedmi et al., 2014; Wang et al., 2014), the most likely candidate is TRF2. Indeed, knockdown of TRF2, but not TRF1, in NSCs also resulted in reduced NSC numbers, smaller NSC lineages and abnormal NSC morphology (Fig. 1D,E; Table S1). Because NSC-TAFs and TRF2 regulate the expression of the type I NSC marker *Ase*, we asked whether they are also important in type II NSCs, which do not express *Ase*. Knockdown of either TBP, TRF2 or TAF9 using a type II NSC driver (UAS-Dicer2; worniuGAL4, aseGAL80; UAS-CD8:GFP) diminished the number of type II NSCs (Fig. 1F,G). Altogether, our genetic analysis using *in vivo* transgenic RNAi demonstrate that a unique subset of TAFs, TBP and TRF2 have distinct and gene-selective functions in the identity of both type I and type II NSCs.

Analysis of *Tbp*, *Trf2* and *Taf* alleles

To corroborate our RNAi results, we assessed the effects of available mutant *Taf* alleles on NSC phenotypes. Because *Tafs* are known or predicted to be essential genes, and loss of *Taf* function in other cellular contexts results in either cell death or cell cycle arrest, we turned again to the MARCM system to analyze NSC clones. In these and subsequent experiments, our choice of which NSC-TAF to analyze was primarily governed by reagent availability. NSC clones that were homozygous mutant for either *Taf4^{LL07382}* (Schuldiner et al., 2008), *Taf7^{LL01754}* (Schuldiner et al., 2008) or *Taf9¹⁹⁰* (Xie et al., 2014) exhibited a marked reduction in clone size, mitotic index and *Ase* levels (Fig. 2C–H). Next, we analyzed the phenotype of a *Tbp* allele, *Tbp^{S110}*, which generates a truncated protein that cannot bind DNA *in vitro* (Hsu et al., 2014). Surprisingly, *Tbp^{S110}* NSC clones were readily recovered, expressed normal levels of *Ase*, but generated fewer cells than the control clones (Fig. 2I,J). We anticipated that *Trf2* mutants would

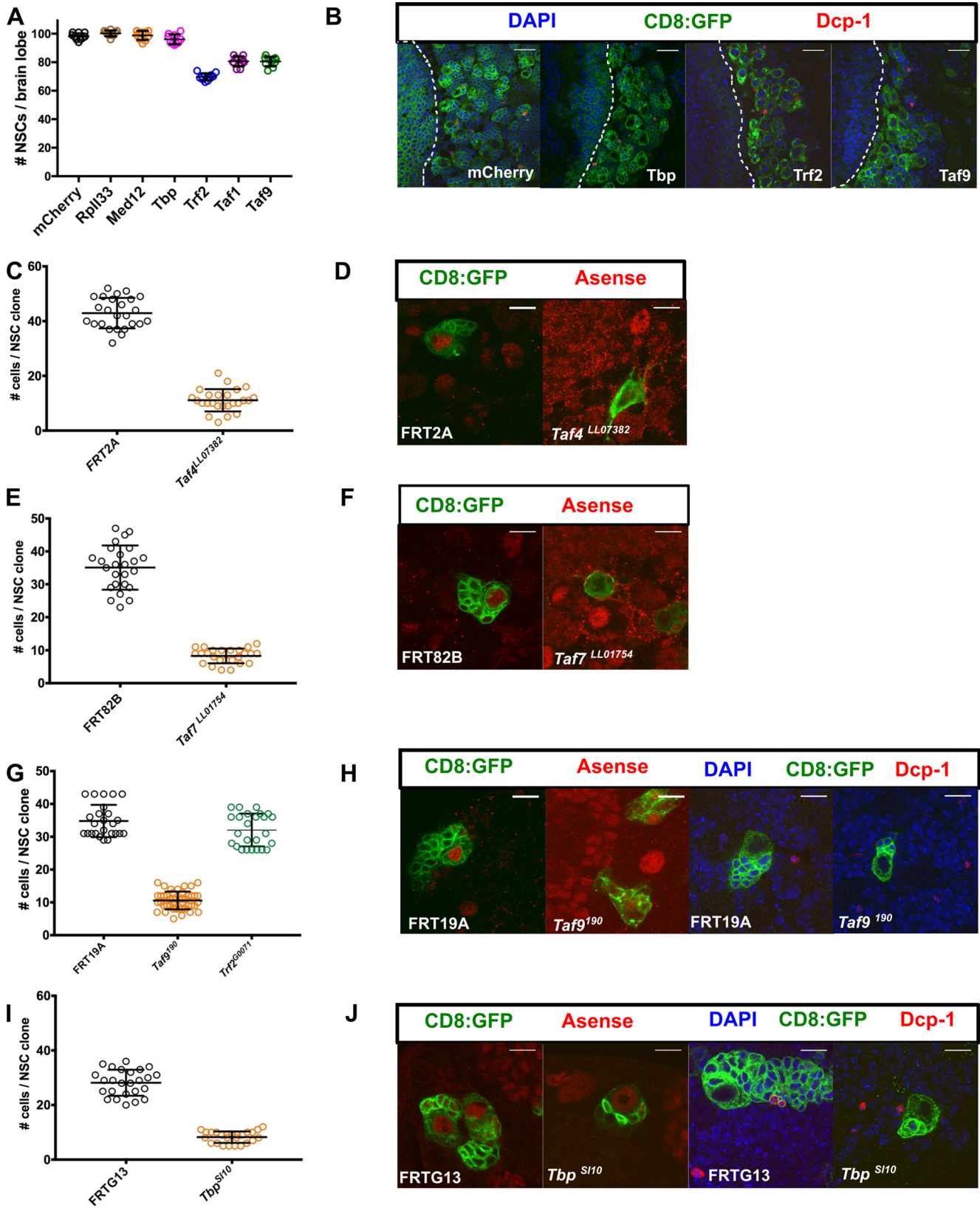


Fig. 2. See next page for legend.

phenocopy the examined *Taf* mutants, yet NSC clones homozygous for a hypomorphic allele, *Trf2*^{G0071}, only exhibited a modest reduction in clone size (Fig. 2G).

The reduced clone size in *Taf4*^{LL07382}, *Taf7*^{LL01754}, *Taf9*¹⁹⁰ or *Tbp*^{S110} NSC clones is indicative of either a delay in cell cycle progression or reduced survival. To distinguish between these

Fig. 2. TBP, TRF2 and NSC-TAFs are required for normal NSC output but not for NSC survival. (A) Blocking apoptosis does not rescue NSC loss observed upon knockdown of TRF2, TAF1 or TAF9. The listed RNAi transgenes were co-expressed with UAS-miRHG, which blocks apoptosis, using a pan-NSC driver (*worniu*GAL4, UAS-GFP). *P*-values were *RpII33* (0.4216), *MED12* (0.9893), *TBP* (0.4710), *TRF2* (<0.001), *TAF1* (<0.001), *TAF9* (<0.001). (B) Knockdown of TBP, TRF2 or TAF9 does not result in cleaved caspase (*Dcp-1*) The white dotted line demarcates the optic lobe (left)/central brain (right) boundary. (C,D) *Taf4^{LL07382}* NSCs generate fewer cells and exhibit decreased *Asense* expression than control clones (*FRT2A*; *P*-value<0.0001). (E,F) *Taf7^{LL07382}* NSCs exhibit a marked decrease in *Asense* expression and generate fewer cells than controls (*FRT2B*; *P*-value<0.0001). (G,H) *Taf9¹⁹⁰* NSCs, but not *Trf2^{G0071}* NSCs, exhibit a marked decrease in *Asense* expression and generate fewer cells than controls (*FRT19A*). *P*-values were *Taf9¹⁹⁰* (<0.0001), *Trf2^{G0071}* (0.0331). (I,J) *Tbp^{S110}* NSC generate fewer cells than control clones (*FRTG13*; *P*-value<0.0001) but maintain *Asense* expression. In C, E and I, experimental clones were compared to the control clones using an unpaired *t*-test. In A and G, experimental clones were compared to control clones using a one-way ANOVA with Dunnett's multiple comparison test. Scale bars: 20 μ m (B); 10 μ m (D,F,H,J).

possibilities, we examined a marker of apoptosis in either NSCs depleted for TBP, TRF2 or TAF9 by RNAi or *Taf4^{LL07382}*, *Taf7^{LL01754}*, *Taf9¹⁹⁰*, *Tbp^{S110}* NSC clones, but did not detect apoptotic NSCs as determined by staining for cleaved caspase (*Dcp-1*; Fig. 2B,H,I) in any of the genotypes examined. To test whether blocking apoptosis affected the observed NSC loss phenotype, we used a microRNA transgene (*miRHG*) that concurrently downregulates three major pro-apoptotic genes in *Drosophila*: *reaper*, *hid* and *grim* (Siegrist et al., 2010). Expression of *miRHG* in NSCs failed to suppress the phenotypes caused by knockdown of TRF2, TAF1 or TAF9 or in NSC clones that were homozygous mutant for *Taf4^{LL07382}* (Fig. 2A, compare with Fig. 1D; Fig. S2B). Importantly, we found that the function of NSC-TAFs and TRF2 in cell survival was context-dependent, as knockdown of TBP, TRF2 or TAF9 resulted in apoptosis when the respective RNAi transgenes were expressed in epithelial cells of the wing disc using an inducible GAL4 driver (*apterous*-GAL4, UAS-GFP; *tubulin*GAL80^{ts}; Fig. S2D).

TBP, TRF2 and NSC-TAFs control NSC proliferation

Because the reduction in NSC lineage size upon NSC-TAF or TRF2 depletion does not appear to be caused by apoptosis, we predicted that NSC-TAF or TRF2 knockdown NSCs would exhibit a cell cycle delay. To directly test this, we performed EdU labeling experiments and found that after a 2 h pulse, *RpII33*, TBP, TRF2, TAF1 and TAF9 knockdown NSCs had fewer EdU⁺ NSCs (Fig. 3A). All genotypes examined also had a lower mitotic index (*pH3*⁺ NSCs/total NSCs; Fig. 3B). Intriguingly, *RpII33* knockdown NSCs presented a more severe proliferation phenotype, suggesting that the severity of cell cycle progression defects don't always correlate with NSC self-renewal. (Fig. 3B). Examination of additional cell cycle markers demonstrated that TAF1 and TAF9 were required for PCNA-GFP expression, whereas only TRF2 was required for high levels of *CycE* expression (Fig. 3E,F). Accumulating evidence from diverse stem cell systems suggest an intricate link between cell cycle progression and stem cell self-renewal. For example, during development of the mouse cerebral cortex, lowering *CyclinD1/Cdk4* expression in NSCs lengthens G1 and results in precocious neurogenesis and similarly, the short G1 phase in murine ESCs has been linked to pluripotency (Lange and Calegari, 2010; Coronado et al., 2013). Because NSC-TAF and TRF2 knockdown NSCs exhibited cell cycle delay,

we hypothesized that they had an extended G1 phase and would be hypersensitive to manipulation of the G1/S transition. To address this, we lowered *CycE/Cdk 2* activity in control or TAF9 knockdown NSCs by overexpressing the CIP/KIP family Cyclin-dependent kinase inhibitor *Dacapo* (*Dap*). We found that *Dap* overexpression had no effect on NSC numbers in a control RNAi background, but further reduced the number of NSCs upon TAF9 knockdown (Fig. 3C). Next, we asked whether this sensitivity was specific to the G1/S transition or if it also applies to the G2/M transition. To this end, we overexpressed *Wee1*, a Ser/Thr kinase that inhibits *Cdk1*, or knocked down *string/cdc25*, a phosphatase and *Cdk1* activator, in either control or TAF9 knockdown NSCs. Again, we found that *Wee1* overexpression or *string/cdc25* knockdown did not result in NSC loss, despite an almost complete block in cell cycle progression. However, in combination with TAF9 knockdown, *Wee1* overexpression or *string/cdc25* loss resulted in a more severe NSC loss relative to TAF9 RNAi alone (Fig. 3D). Finally, we asked whether TBP, TRF2 or TAF9 knockdown NSCs exhibited a lengthening of the G1 phase of the cell cycle using the Fly-FUCCI system, a dual color fluorescent reporter for cell cycle stages (Zielke et al., 2014). We further distinguished G2 cells (*GFP*⁺, *RFP*⁺, *pH3*⁻) from cells in mitosis (*GFP*⁺, *RFP*⁺, *pH3*⁺) by staining with the mitotic marker *pH3*. Surprisingly, we found that the majority of both control and experimental NSCs were in G2 (Fig. 3G). Taken together, our results show that NSC-TAFs regulate multiple aspects of NSC cell cycle progression and that depletion of either NSC-TAFs or TRF2 renders NSCs hypersensitive to both G1/S and G2/M cell cycle manipulation.

Regulation of NSC cell polarity and differentiation by TBP, TRF2 and NSC-TAFs

NSC cell polarity is required for asymmetric segregation of cell fate determinants and NSC self-renewal. To address whether the NSC-TAFs and TRF2 phenotypes involve defects in cell polarity, we examined the expression and localization of key polarity proteins that are inherited by the daughter NSC. We found that both interphase and mitotic NSCs that were homozygous mutant for either *Taf4^{LL07382}* or *Taf7^{LL01754}* failed to express normal levels of *Inscuteable* (*Insc*) (Fig. 4A,B). We next examined the localization of atypical protein kinase C (*aPKC*) in *pH3*⁺ NSCs. In 23/24 of control NSCs (*mCherry*), *aPKC* exhibited a strong cortical crescent. In contrast, only 13/19 of TBP knockdown NSCs, 14/20 TRF2 knockdown NSCs or 5/13 TAF9 knockdown NSCs properly localized *aPKC* during mitosis (Fig. S4B).

To ascertain if knockdown of NSC-TAFs or TRF2 results in premature differentiation, we examined the expression of both *Pros* – a homeodomain transcription factor that is necessary and sufficient for differentiation of type I NSCs (Choksi et al., 2006) – and *Elav*, a conserved RNA-binding protein that is expressed in post-mitotic neurons. Neither wild-type NSCs nor NSCs that were depleted for TBP, TRF2 or TAF9 by RNAi or *Taf4^{LL07382}*, *Taf7^{LL01754}*, *Taf9¹⁹⁰* homozygous mutant NSCs expressed either *Pros* or *Elav* in their nuclei (Fig. 4C,D; Fig. S4C). Moreover, our RNA-seq analysis, described in more detail below, showed that the levels of *pros* and *elav* transcripts were reduced in TAF9-depleted NSCs whereas *pros* but not *elav* transcripts were reduced in either TRF2-depleted or TBP-depleted NSCs. We conclude that NSCs lacking NSC-TAF or TRF2 exhibit defective NSC cell polarity but unlike other NSC identity genes, do not appear to undergo *Pros*- or *Elav*-mediated premature differentiation (Lai et al., 2012; Rust et al., 2018).

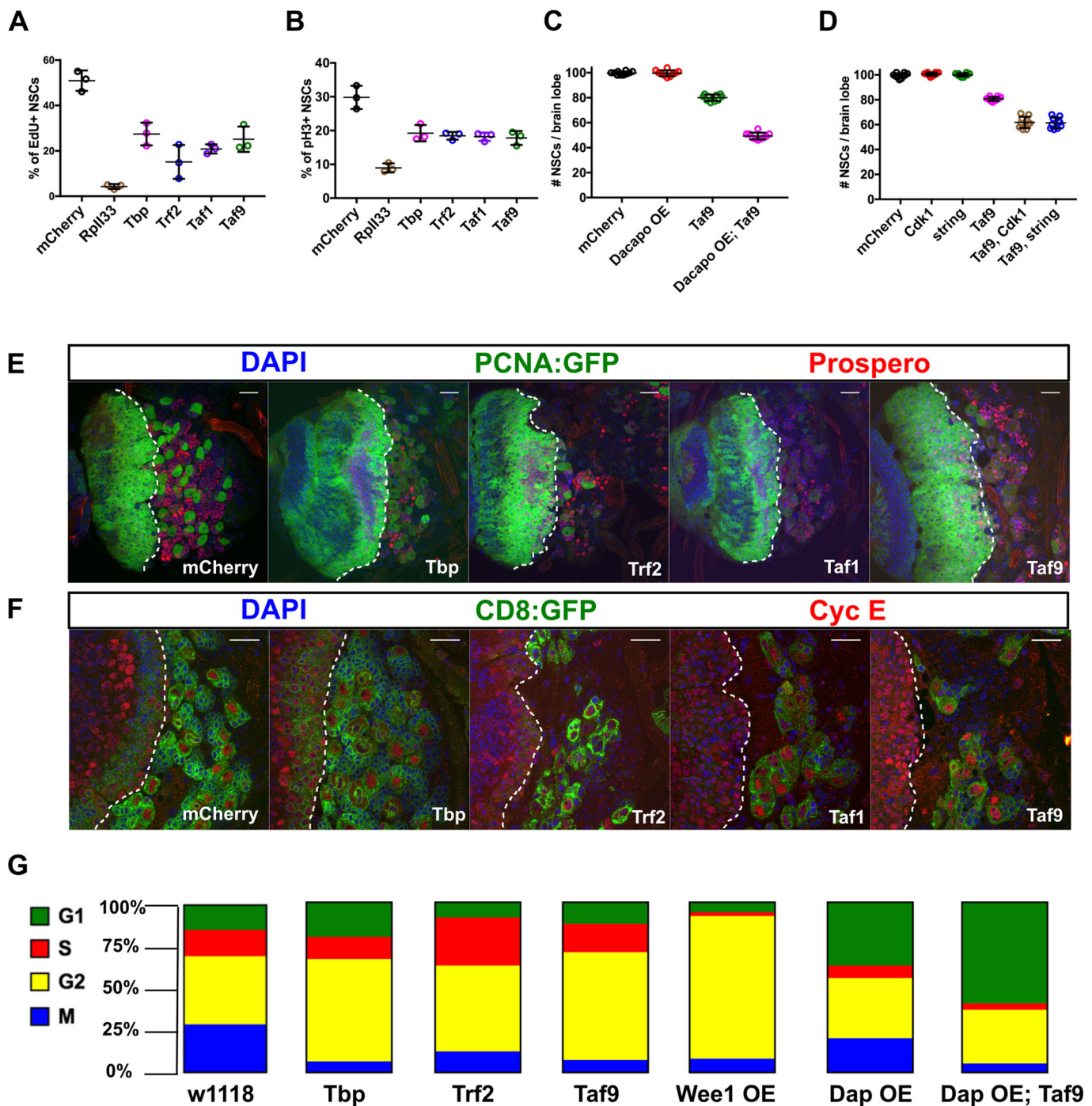


Fig. 3. TBP, TRF2 and NSC-TAFs are required for NSC cell cycle progression. (A) Quantification of percentage of NSCs that incorporated the thymidine analog EdU after a 2 h pulse. *P*-values were Rpll33 (<0.0001), TBP (0.0003), TRF2 (<0.0001), TAF1 (<0.0001), TAF9 (0.0001). (B) Quantification of percentage of NSCs that are positive for the mitotic marker phospho Histone H3 (pH3). *P*-values were Rpll33 (<0.0001), TBP (0.0002), TRF2 (0.0001), TAF1 (<0.0001), TAF9 (0.0001). (C) Quantification of NSCs in nervous systems expressing the listed RNAi or overexpression transgenes. *P*-values were Dacapo overexpression (0.9994), TAF9 (<0.0001), TAF9, Dacapo overexpression (<0.0001). (D) Quantification of NSCs in nervous systems expressing the listed RNAi transgenes. *P*-values were Cdk1 (0.8166), string (0.9871), TAF9 (<0.0001), TAF9, Cdk1 (<0.0001), TAF9, string (<0.0001). (E) Brain lobe images of nervous systems expressing the listed RNAi transgenes, the cell cycle marker PCNA-GFP (Green) and Prospero (Red). (F) Single confocal sections of nervous systems expressing the listed RNAi transgenes and the cell cycle marker Cyclin E. In E and F, the white dotted line demarcates the optic lobe (left)/central brain (right) boundary. (G) Analysis of cell cycle phasing with the Fly-FUCCI system. In A–F transgenes were expressed with a pan-NSC driver (worniuGAL4, UAS-GFP) and experimental genotypes were compared to the mCherry control using a one-way ANOVA with Dunnett's multiple comparison test. In G, UAS transgenes were driven by a pan-NSC driver combined with the Fly-FUCCI cassette (worniuGAL4; UASp-GFP.E2f1.1-230, UASp-mRFP1.CycB.1-266/TM6B).

Identification of TBP, TRF2 and NSC-TAF regulated genes

Because the NSC-TAF and TRF2 phenotypes were similar, we hypothesized that NSC-TAFs and TRF2 co-regulate a subset of

NSC-expressed genes that in turn are collectively required for NSC identity, and that these NSC-TAF-TRF2 co-regulated genes are distinct from NSC-TAF-TBP-regulated genes. Several lines of

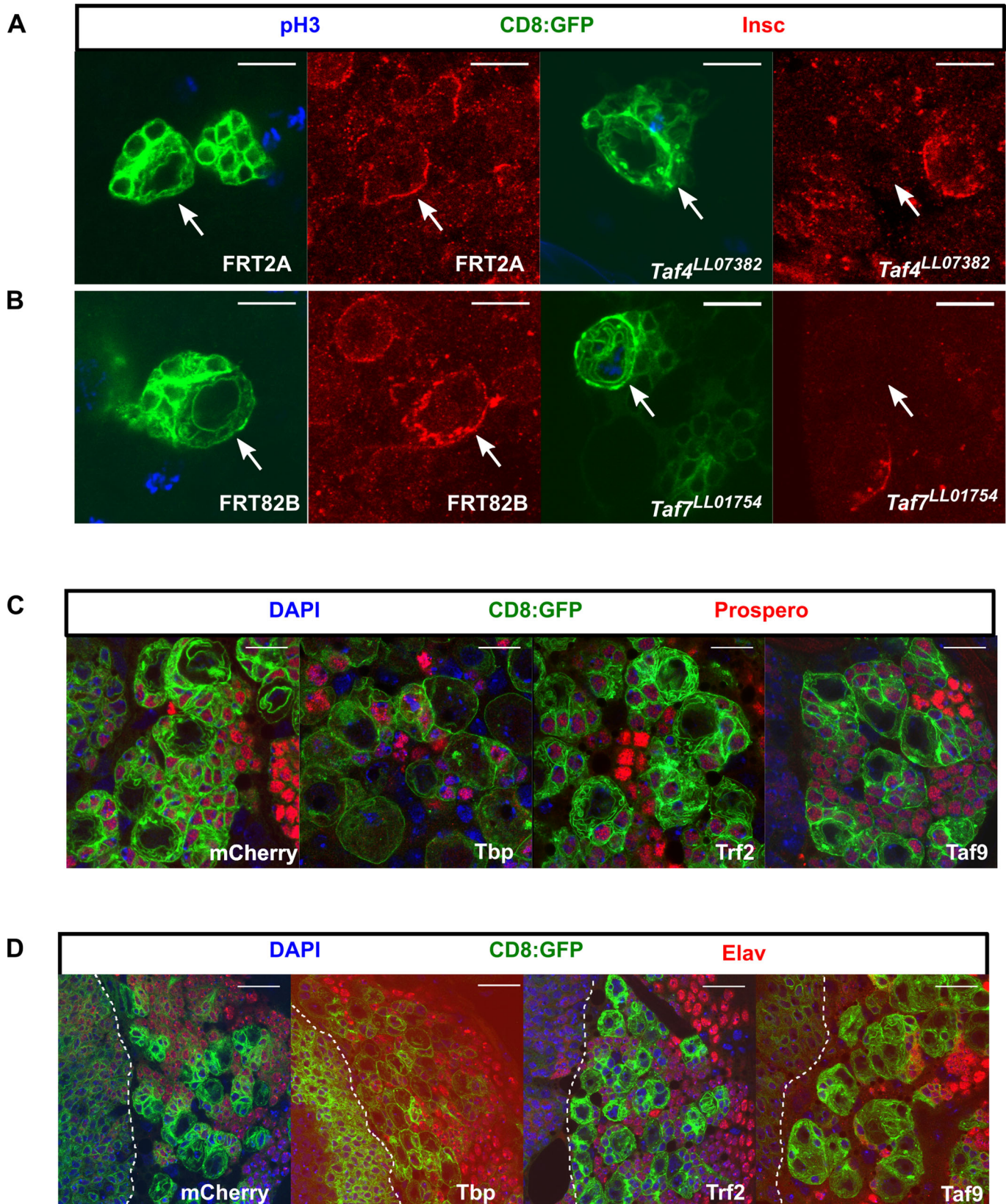


Fig. 4. NSC-TAF or TRF2-depleted NSCs exhibit defective cell polarity but do not express differentiation markers. (A) *Taf4^{LL07382}* NSCs or (B) *Taf7^{LL07382}* NSCs fail to express normal levels of Insc. Mitotic cells are labeled with phospho Histone H3 (pH3), CD8:GFP (a membrane-tethered GFP) labels the clones and Insc is shown in red. (C) Knockdown of TBP, TRF2 or TAF9 does not result in nuclear accumulation of Prospero. (D) Knockdown of TBP, TRF2 or TAF9 does not result in nuclear accumulation of Elav. The white dotted line demarcates the optic lobe (left)/central brain (right) boundary. In both C and D, transgenes were expressed using a UAS-Dcr2; *inscGAL4*, UAS-CD8:GFP, tubGAL80^{ts} driver and transgenes induced for 72 h. Scale bars: 10 μm (A–C); 20 μm (D).

evidence suggest that changes in abundance of NSC-TAFs, TBP and TRF2 alone are unlikely to explain their NSC-selective functions. First, we found that TBP, TAF1, TAF4 and TAF12 proteins are not restricted to NSCs and are expressed ubiquitously in the brain (Fig. S3A–C). We corroborated and extended these observations by mining a published RNA-seq data set, which revealed that TBP, TRF2 and NSC-TAFs are all expressed at comparable levels in FACS-purified NSCs and FACS-purified neurons (Berger et al., 2012). Second, recent RNA-seq data derived from robotically-sorted NSCs revealed that TRF2 and TAF4 were among a group of 61 transcription factors highly expressed in multiple NSC lineages (Yang et al., 2016). Therefore, we reasoned that understanding how NSC-TAFs and TRF2 regulate NSC identity requires the identification of NSC-specific transcriptomes. To identify genes co-regulated by NSC-TAFs and TRF2, we performed RNA-seq analysis of FACS-purified NSCs expressing either control (mCherry), TBP, TRF2, or TAF9 RNAi transgenes in type I NSCs, driven by a type I specific driver (asenseGAL4, Stinger:GFP). Compared to the mCherry control, and defining differentially expressed genes (DEGs) as those that exhibited a log₂ fold change >1 and False Discovery Rate (FDR) <0.05, we identified 2776 DEGs in the TBP RNAi (Fig. 5A, left; Table S2), 152 upon TRF2 knockdown (Fig. 5A, center; Table S3) and 1165 in the TAF9 RNAi (Fig. 5A, right; Table S4). Because core promoter factors are required for transcriptional activation, we focused on the downregulated genes. Unexpectedly, most of the 1488 TBP-dependent genes were private (i.e. not co-regulated by TRF2 or TAF9), but 119 of these also overlapped with 587 genes downregulated upon TAF9 knockdown and this overlap was statistically significant ($P=8.98 \times 10^{-23}$, hypergeometric test; Fig. 5B). Of the 94 downregulated genes in the TRF2 RNAi condition, 45 also required TAF9 for their expression ($P=6.08 \times 10^{-60}$, hypergeometric test). Gene ontology (GO) analysis revealed that TBP-dependent genes were enriched for several mRNA metabolic processes and cell cycle regulation, whereas the TAF9 regulated genes were enriched for GO terms related to regulation of gene expression and transcription, as well as stem cell differentiation (Fig. 5E; Tables S5 and S6). In contrast, the TRF2-dependent genes did not present enriched GO categories after correcting for multiple hypothesis testing. Strikingly, the majority of TAF9-dependent genes were also private (i.e. not co-regulated by TRF2 or TBP), and included known NSC polarity genes (*insc*, *numb*, *pun*), NSC transcription factors (*HmgD*, *klu*, *chinmo*, *kni*) and the neuronal marker (*elav*).

For simplicity, we refer to the TBP-TAF9 co-regulated genes as NSC-TAF-TBP-dependent genes. Intriguingly, amongst the NSC-TAF-TBP targets were genes known to be involved in NSC fate determination and asymmetric cell division (*mira*, *brat*, *pon*, *pros*), cell cycle genes (*E2F1*, *CycE*, *stg*; Fig. S5C), regulators of NSC temporal identity (*Syp*, *svp*) as well as several transcription factors (*sqz*, *nab*, *foxo*, *Mnt*, *tap*) and genes encoding RNA-binding proteins (*Rsf1*, *Hrb87F*, *B52*, *U4-U6-60K*; Fig. 5D; Fig. S5D). We refer to genes that required both TRF2 and TAF9 for their expression as NSC-TAF-TRF2 targets. Many of these genes also encode transcription factors (*dati*, *hng3*, *HmgZ*, *mamo*, *Hr4*, *bi*, *jim*) and RNA-binding proteins (*shep*, *bru3*, *aub*, *pum*). We next performed an unbiased motif discovery of cis-regulatory sequences enriched in the TBP, TRF2 and TAF9 target genes using HOMER and unexpectedly, we found that all three sets of target genes were enriched for E-boxes, the DNA replication-related element (DRE) as well as some orphan motifs (Fig. 5C). Taken together, our RNA-seq analysis revealed a complex regulatory network

orchestrated by different sets of core promoter factors, with NSC-TAF-TBP regulated genes involved in cell cycle progression, NSC polarity and fate determination, whereas NSC-TAF-TRF2 targets encode a set of transcription factors and RNA-binding proteins distinct from the NSC-TAF-TBP targets.

Identification of TBP, TRF2S and TAF5 genomic binding sites

To test whether NSC-TAFs and TRF2 co-occupy a subset of target genes that are distinct from TFIID-regulated genes identified in our RNA-seq experiments, we profiled the genomic binding sites of TBP, TRF2S and a representative NSC-TAF (TAF5) using the targeted DamID (TaDa) system (Southall et al., 2013). Using this system, we drove expression of UAS-Dam, UAS-Dam-TBP, UAS-Dam-TRF2S and UAS-Dam-TAF5 using a *worniuGAL4*, UAS-GFP, *tubGAL80^{ts}* driver and a 72 h induction period. We identified the methylated GATC sites identified by next-generation sequencing and by using the parameters described in the Materials and Methods section, we identified 3100 peaks for Dam-TBP, 3028 for Dam-TRF2S and 3659 for Dam-TAF5. As expected, these peaks were significantly over-represented at and around transcription start sites (TSS; Fig. 6A,B). Analysis of over-represented motifs surrounding TSS-associated peaks with HOMER revealed that DRE motifs, E-boxes and an Initiator-like sequence were enriched in all three Dam fusion proteins (Fig. 6D). To determine which genes are co-bound by the three Dam fusion proteins, we selected all peaks that were annotated as promoter/TSS and asked to what extent they overlap. As shown in the Venn diagram in Fig. 6C, a significant number of bound genes are shared between the three Dam fusion proteins. Importantly, analysis of peaks identified in both replicates produced a similar picture (Fig. S6). Consistent with our RNA-seq analysis, 955 of the TSS-associated peaks were shared between Dam-TBP and Dam-TAF5, whereas 506 peaks were shared between Dam-TAF5 and Dam-TRF2S. Moreover, this analysis also showed that Dam-TAF5 and Dam-TBP co-bound to the promoter/TSS of several of NSC-TAF-TBP-dependent genes identified above, including transcription factors (*sqz*, *nab*, *foxo*, *Mnt*, *tap*), cell cycle genes [*E2F1*, *CycE* (Fig. 7A), *stg*] and RNA-binding proteins [*Syp* (Fig. 7B), *Rsf1*, *Hrb87F*, *B52*, *U4-U6-60K*]. However, the Dam-TAF5 and Dam-TRF2S co-bound genes included those encoding transcription factors (*dati*; Fig. 7B, *mamo*, *Hr4*) and the RNA-binding protein *bru-3* (Fig. 7C). Strikingly, some of the TAF9-dependent genes that did not require TBP for their expression were nonetheless co-bound by Dam-TAF5 and Dam-TBP, including *klu* (Fig. 7D) and *insc* (Fig. 7E). Taken together, the gene ontology and motif analysis of our RNA-seq data, combined with identification of genomic binding sites for this network of core promoter factors using DamID-seq, support the notion that NSC-TAF complexes directly regulate multiple aspects of NSC identity, including NSC cell polarity, cell cycle progression and RNA metabolism.

DISCUSSION

Control of developmental gene expression is thought to rely on the combinatorial action of gene-specific transcription factors. The concerted action of activators and repressors is thought to ultimately converge on a highly conserved general transcription factor, TFIID. Based on studies in yeast and cultured mammalian cells, TFIID, composed of TBP and 13 TAFs, has been historically considered to be an essential yet passive player in gene regulation. However, the emergence in metazoans of both TBP and TAF paralogs, and of additional core promoter elements, has been proposed to contribute to the evolution of bilaterians by supporting

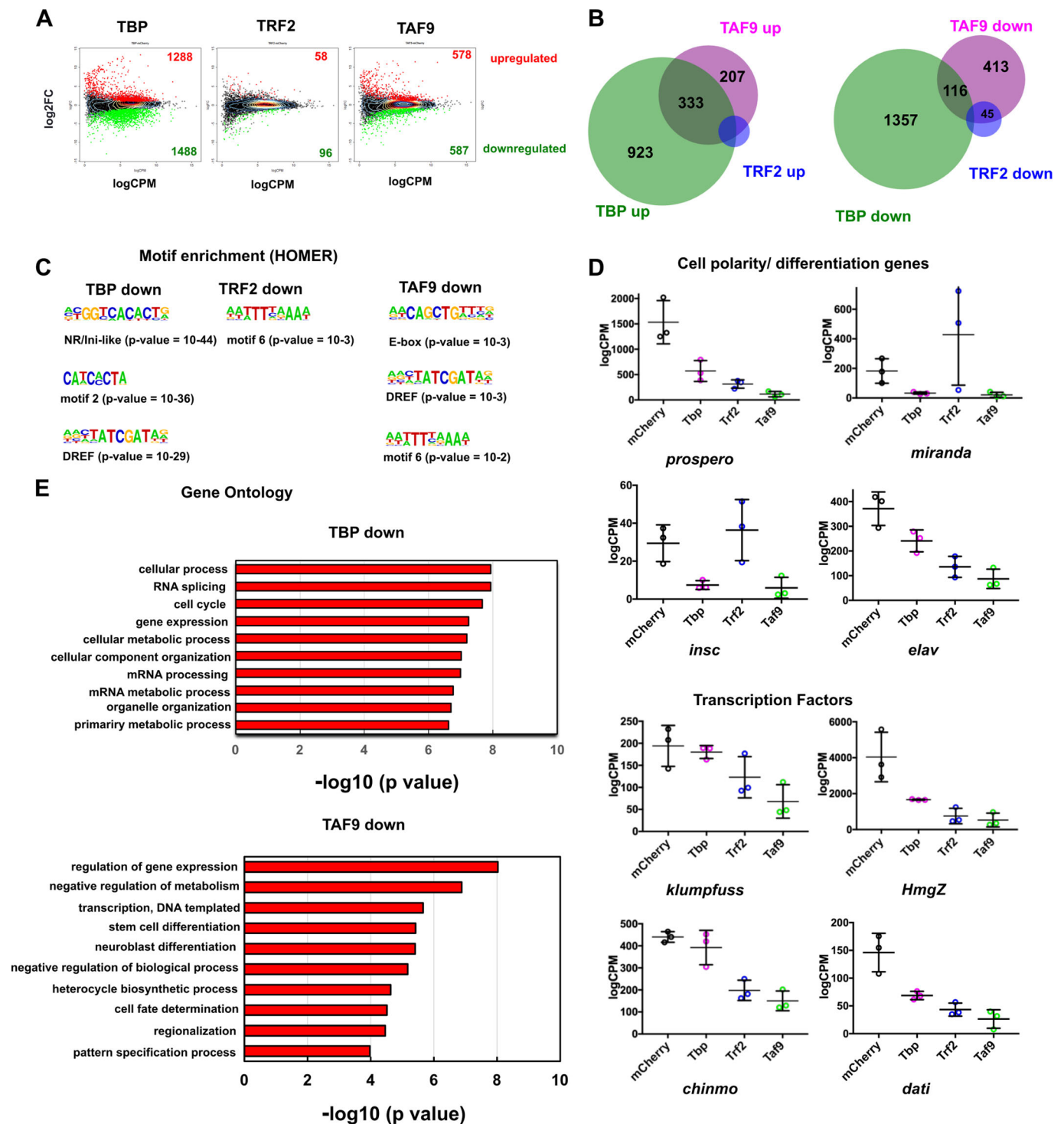


Fig. 5. Identification of TBP, TRF2 and NSC-TAF target genes. (A) MA-plots of RNA-seq analysis and identification of differentially expressed genes (DEGs). The numbers of upregulated and downregulated genes are shown in red and green, respectively. (B) Venn diagrams show the overlap between upregulated genes (left) or downregulated (right) DEGs identified for TBP (green), TRF2 (blue) and TAF9 (magenta). (C) Motif analysis of downregulated genes using HOMER. (D) Normalized read counts of selected target genes. (E) Selected gene ontology categories that are over-represented in gene sets downregulated upon TBP (top) or TAF9 knockdown (bottom).

more complex transcriptional programs (Duttke et al., 2014). Evidence from genetic and biochemical studies in a wide variety of model systems suggest that this diversity has indeed allowed multiple TAFs to take on cell- or tissue-specific functions. For example, the TAF9 paralog TAF9B regulates neuronal gene expression by associating with the SAGA/PCAF co-activator

complex, whereas the TAF7 paralog TAF7L associates with TBP-related factor 2 (TRF2) to direct expression of a subset of post-meiotic genes during spermiogenesis (Herrera et al., 2014; Zhou et al., 2013). However, these examples are generally restricted to orphan TAFs, while prototypical TAFs are primarily present in TFIID and/or SAGA complexes.

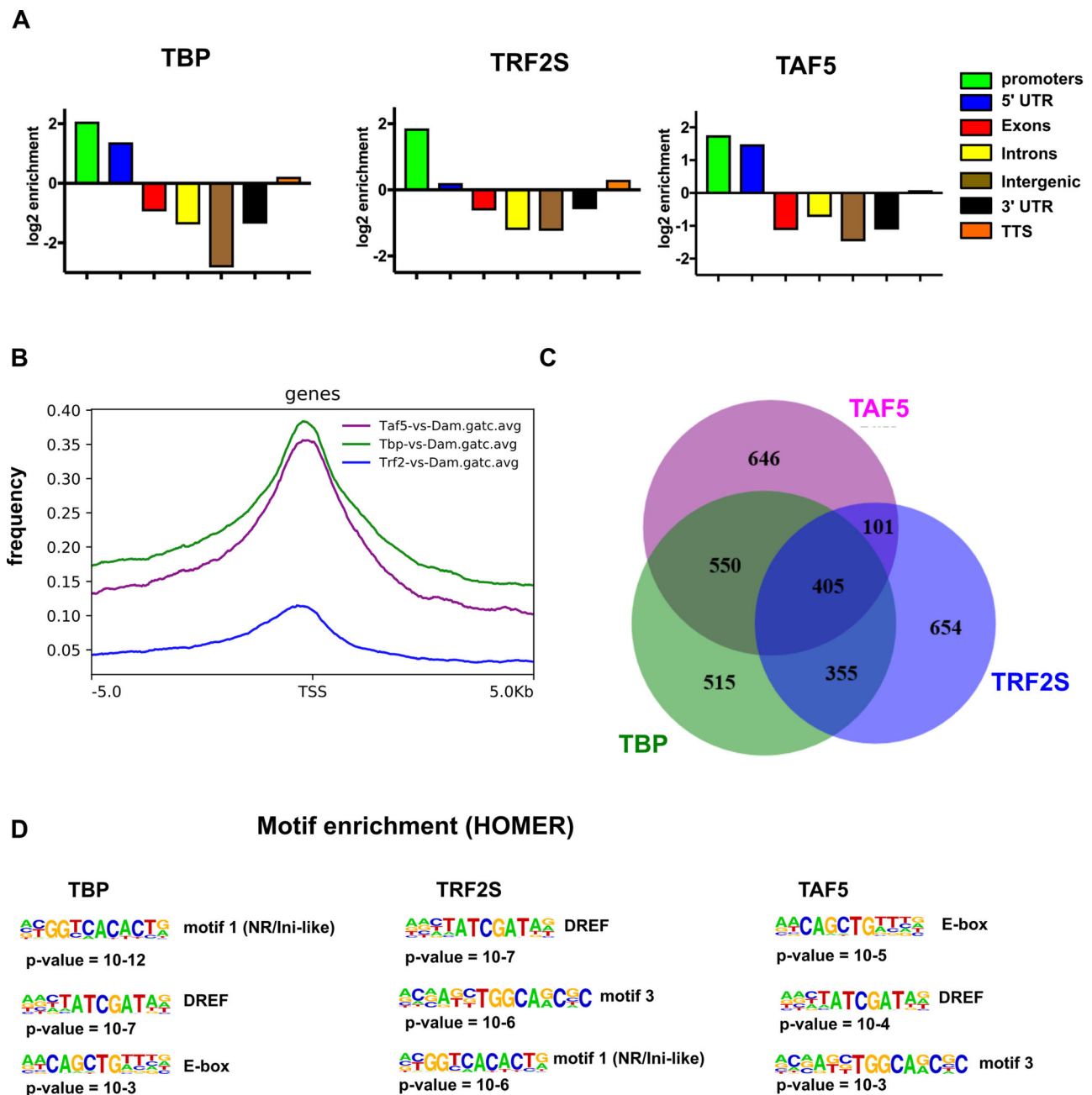


Fig. 6. Identification of bound genomic regions by DamID-seq. (A) Genomic distribution of regions bound by Dam-TBP, Dam-TRF2S and Dam-TAF5 shows enriched binding at promoters and 5'UTRs. Plots show log₂ enrichment scores (observed/expected). (B) Metagenome profile of DamID-seq data for Dam-TBP (green), Dam-TRF2S (blue) and Dam-TAF5 (magenta). (C) Venn diagram showing the statistically significant overlap between genes with TSS-associated peaks. (D) Motif enrichment analysis of peaks identified motifs similar to those identified in the RNA-seq analysis.

In this study, using *Drosophila* NSCs as a model, we uncovered gene-selective functions for a subset of TAFs, NSC-TAFs, and some of these functions are shared with TRF2 whereas others are shared with their canonical binding partner, TBP. Our finding that NSC-TAFs did not regulate survival was unexpected, as deletion of *Taf9* in chicken DT40 cells, of *Taf4a* in mouse embryos or TAF9 depletion in wing disc epithelial cells all result in increased apoptosis (Chen and Manley, 2000; Langer et al., 2016; Xie et al., 2014). However, it's unclear whether TAFs are required for survival of embryonic stem cells (ESCs) as inducible depletion of TAF8 resulted in ESC cell death in one study whereas no cell death was detected upon knockdown of either TAF5 or TAF6 in a different study (Pijnappel et al., 2013; El-Saafin et al., 2018). In contrast to a report

using murine ESCs (Pijnappel et al., 2013) in which a stable TAF5 knockdown ESC line prematurely differentiated without affecting the cell cycle, we show here that NSC-TAFs and TRF2 control stem cell identity in part, through direct regulation of the cell cycle. Depletion of NSC-TAFs or TRF2 by RNAi diminished the number of NSCs that incorporated the thymidine analog EdU, lowered the mitotic index, and rendered NSCs hypersensitive to cell cycle manipulation. Moreover, we identified DamID peaks at key cell cycle genes, including *E2F1*, *CycE* and *string*. We initially hypothesized that NSCs depleted for NSC-TAFs or TRF2 would both exhibit an extended G1 phase and be hypersensitive to manipulation of the G1/S transition. However, quantification of cell cycle phases using a FUCCI-based reporter showed that NSCs depleted for NSC-TAFs or

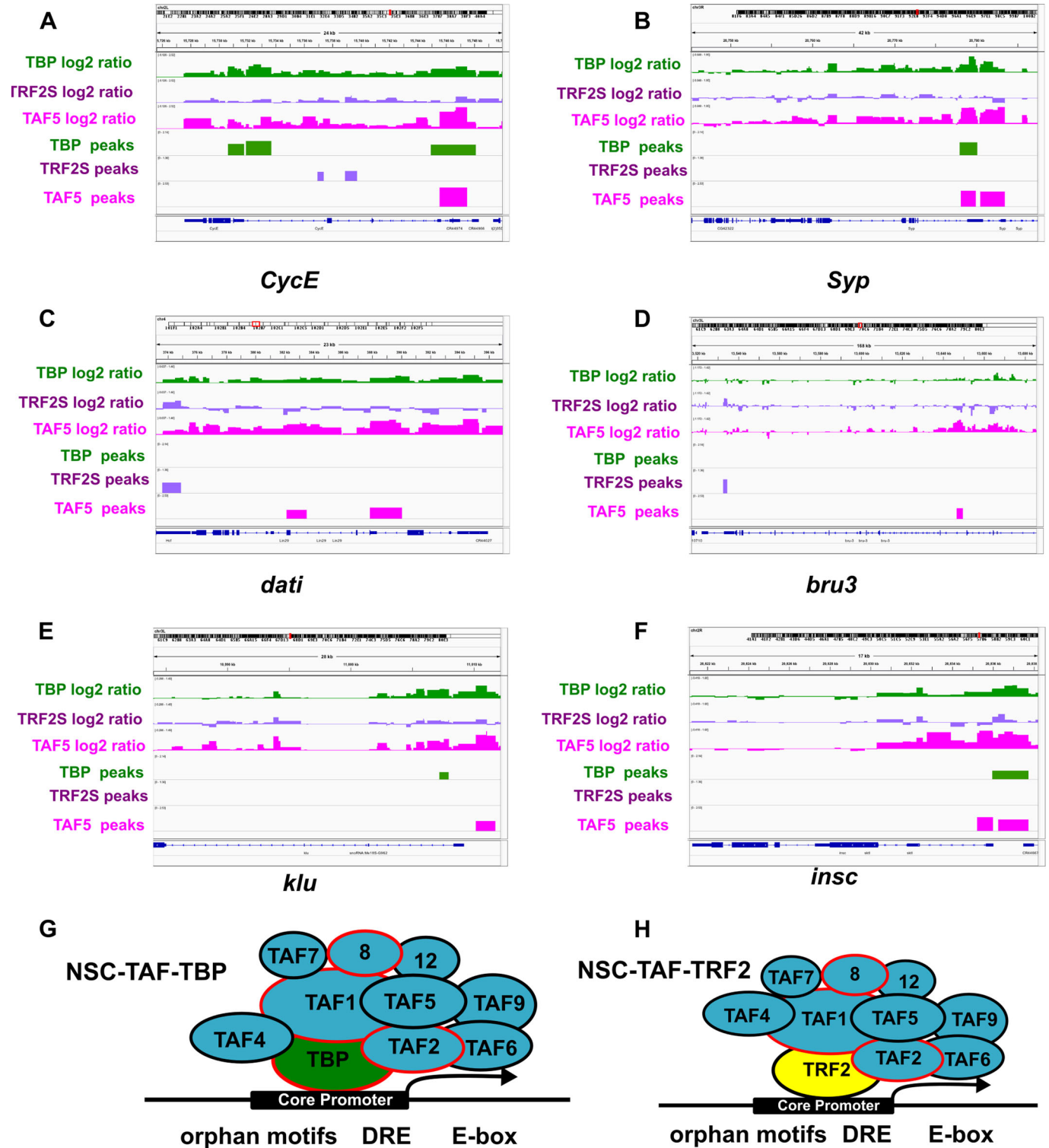


Fig. 7. Model for regulation of TBP, TRF2 and NSC-TAF target genes. (A–F) Screenshots of DamID-seq tracks showing the log₂ ratios for both replicates and identified peaks for TBP (green), TRF2S (purple) and TAF5 (magenta) for *CycE* (A), *Syp* (B), *dat1* (C) and *bru3* (D), *klu* (E) and *insc* (F). (G) A putative NSC-TAF-TBP complex regulates a subset of NSC-expressed genes that enriched for DREs, E-boxes and orphan motifs. (H) A putative NSC-TAF-TRF2 complex regulates a different subset of NSC-expressed genes that are also enriched for DREs, E-boxes and orphan motifs.

TRF2 were in fact primarily in G2 and exhibited hypersensitivity to manipulation of both the G1/S and G2/M transitions. Intriguingly, a recent study showed that quiescent NSCs, which are known to extend a primary process, arrest primarily in G2 and are labeled by *tribbles* (*trbl*), which encodes a conserved pseudokinase (Chell and Brand,

2010; Otsuki and Brand, 2018). These phenotypes are remarkably similar to those observed upon depletion of NSC-TAFs or TRF2 and we note that the *trbl* locus is occupied by TBP, TRF2S and TAF5.

Because NSC-TAFs and TRF2 exhibit similar loss of function phenotypes and share at least 45 target genes in addition to the type I

NSC marker *ase*, we proposed that they function together to direct expression of a subset of NSC-expressed genes (Fig. 7H). We tested this hypothesis by combining expression analysis using RNA-seq of FACS-purified NSCs and by determining the genomic binding sites for TBP, TRF2S and a representative NSC-TAF (TAF5), using Targeted DamID (TaDa). Our RNA-seq experiments revealed that many genes co-regulated by TBP and TAF9 are known or predicted to be important for NSC identity including the chromatin remodeler *domino* (Rust et al., 2018), the cell cycle genes *E2F1*, *CycE* (Fig. 7A) and *string* and the temporal identity factors *Syp* (Fig. 7B) and *svp*. However, the functional relevance of the NSC-TAF-TBP target genes remains to be determined. Similarly, TAF9-dependent genes that were unaffected upon TBP knockdown and that are bound by TAF5 are good candidates for mediating NSC-TAF's function in self-renewal, such as the transcription factors Chinmo, Klumpfuss (Berger et al., 2012), HmgD and the polarity protein Insc (Fig. 7F). Lastly, while the function of the transcription factors (*dati*, *hng3*, *HmgZ*, *mamo*, *Hr4*, *bi*, *jim*) that are co-regulated by TRF2 and TAF9 and co-occupied by TRF2S and TAF5 are not well characterized, *Dati* (Fig. 7C), *Jim* and *Mamo* have recently been identified as important components of gene regulatory networks uncovered in a single-cell RNA-seq atlas of the adult *Drosophila* brain (Davie et al., 2018).

Because TRF2 neither binds the TATA box nor has sequence-specific DNA binding activity, how does the putative NSC-TAF-TRF2 complex recognize its target genes? Several lines of evidence suggest that DREF, which directly binds the DRE element, could be part of the DNA-targeting mechanism. First, depletion of DREF also results in fewer NSCs and smaller NSC lineages (Neumüller et al., 2011). Second, DREF is known to be part of the TRF2 complex (Hochheimer et al., 2002). Third, motif analyses with HOMER revealed that the DRE was over-represented in peaks identified by TaDa for all three fusion proteins. While a TRF2 complex larger than 500 kDa has been purified from embryonic nuclear extracts, none of the identified TRF2-binding proteins were TAFs (Hochheimer et al., 2002). However, a more recent identification of TRF2S-binding proteins from ovary lysates identified several TAFs (Andersen et al., 2017), raising the possibility that NSC-TAFs and TRF2 form a complex *in vivo*.

While depletion of TBP did not result in loss of *Ase* expression, nor diminish the number of NSCs, we found that TBP was essential for NSC cell cycle progression and directly regulated expression of many cell cycle genes. Intriguingly, knockdown of the RNA Pol II subunit RplI33 resulted in a more severe cell proliferation phenotype than TBP knockdown (Fig. 3A,B) but we note that a complication of the RNAi experiments is that TBP depletion reduced expression of UAS transgenes including the RNAi transgene itself whereas TRF2 or NSC-TAF depletion increased expression of UAS transgenes. However, given the lack of NSC loss in TBP-depleted brains, we were surprised to find that more than a third of NSC-expressed genes detected by our low-input RNA-seq were affected upon TBP knockdown. This is even more striking considering the fact that several NSC-TAFs (TAF1, TAF4, TAF8 and TAF9) were among the genes downregulated upon TBP depletion yet the NSC-TAF and TBP phenotypes are clearly different. Importantly, a study that sought to model the human neurological disorder SCA17 in *Drosophila* showed evidence that TBP is required for normal brain function, as removal of one copy of *Tbp* recapitulates some features of SCA17, such as impaired motility and age-dependent accumulation of vacuoles in the brain (Hsu et al., 2014).

We reasoned that the subset of TAFs that we identified is unique, as it is distinct from any previously described TAF complex. For example,

NSC-TAFs partially overlap with a subset of TAFs that appear to co-regulate the size and composition of lipid droplets in the *Drosophila* fat body with TRF2 (Fan et al., 2017), yet that study did not identify lipid droplet functions for TAF2, TAF7 or TAF8, which are NSC-TAFs. Similarly, in mouse ESCs TFIID was proposed to be integral to the pluripotency circuitry (Pijnappel et al., 2013) yet depletion of two NSC-TAF orthologs (TAF7 or TAF8) did not affect ESCs identity.

Recent exome sequencing studies have produced compelling evidence that pathogenic variants in *TAF1*, *TAF2*, *TAF8* and *TAF13* are linked to intellectual disability and microcephaly (O'Rawe et al., 2015; Hellman-Aharony et al., 2013; El-Saafin et al., 2018; Tawamie et al., 2017). However, none of these variants have been modeled *in vivo*, in part due to a gap in our understanding of the function of TAFs during brain development. By demonstrating that TAFs are required for NSC cell cycle progression, NSC cell polarity, and act to prevent premature differentiation while not affecting survival, our work provides a foundation for future studies aimed at uncovering the causative variants in these disorders (Şentürk and Bellen, 2017).

MATERIALS AND METHODS

Fly stocks

Unless noted otherwise, all flies were raised on standard medium at 25° and expression of UAS transgenes performed at 29°. For the focused RNAi screen, 10–15 virgin females from a tester strain (wormiuGAL4, UAS-GFP, UAS-Dicer2; this study) were crossed to five males from individual RNAi lines obtained from either the Vienna *Drosophila* Resource Center or the Bloomington Stock Center (TRiP lines). List of all RNAi lines used can be found in Table S1. F1 progeny from this cross were raised at 29° and dissected nervous system were screened for changes in the intensity and/or pattern of the GFP signal. Other fly lines used were:

GAL4 drivers

wormiu-GAL4, UAS-GFP; UAS-Dcr-2, apterousGAL4, tubGAL80^{ts} (Li et al., 2013), UAS-Dicer2 (Dietzl et al., 2007); wormiuGAL4, *ase*GAL80; UASCD8:GFP (Chris Doe, University of Oregon, HHMI), *ase*GAL4, Stinger:GFP and UAS-Dicer2; *insc*GAL4, UAS-CD8:GFP; tubGAL80^{ts} (Catarina Homem, CEDOC, Portugal), wormiuGAL4, tubGAL80^{ts}, UAS-GFP/CyO; UAS-flp, act5C>CD2>GAL4/TM6B (this study), wormiuGAL4; UASp-GFP.E2f1.1-230, UASp-mRFP1.CycB.1-266/TM6B (this study).

Mutants

Taf4^{LL07382} (142-038), *Taf7*^{LL01754} (140-455), *Taf13*^{LL04552} (141-287) and *Trf2*^{G0071} were obtained from the Kyoto Stock Center. *e(y)1/Taf9*¹⁹⁰ (Wu-Min Deng; Xie et al., 2014), *Tbp*^{S110} (Spyros Artavanis-Tsakonas; Verheyen et al., 1996), *Taf1*^{M1}, *Taf1*^{M5} (Qinghua Liu; Liang et al., 2015) are published stocks sent by the corresponding authors. We recombined *Tbp*^{S110} onto a FRTG13 chromosome using standard fly genetics.

Transgenes

UAS-Dcr-2 (Dietzl et al., 2007), PCNA-GFP (Thacker et al., 2003), UAS-string RNAi (GL00513), UAS-Dacapo, UAS-Wee1 (Price et al., 2002), UAS-TRF2S-mCherry; (Gibert and Karch, 2011) Jean-Michel Gibert, TAF1-EGFP-FIAsH-StrepII-TEV-3xFlag (BL64451), UAS-TAF2-HA; (Schertel et al., 2013) Konrad Basler, FlyORF, UAS-TAF5-HA (Schertel et al., 2013) Konrad Basler, FlyORF, UAS-FLAG-TRF2S, UAS-TRF2L, UAS-TAF9 (Fan et al., 2017), *Taf12*:2XTY1-SGFP-V5-preTEV-BLRP-3XFLAG (VDRC 318745). The UAS-TRF2S-mCherry, UAS-TAF2-HA and UAS-TAF5-HA lines contained a 3xP3-RFP transgene in the insertion site that was removed by crossing to a Cre-expressing line (Bloomington stock number 34516).

MARCM

FRT19A, *ywhsflp*¹²², tub-Gal80; tub-GAL4, UAS-GFP/MKRS (Laura Buttitta, University of Michigan), w, C155-GAL4, UAS-mCD8-GFP, *hsflp*; FRT40A, tub-GAL80 (Liqun Luo, Stanford University), w, C155-GAL4,

UAS-mCD8-GFP, hsf1p; FRTG13, tub-GAL80 (Liquan Luo), w, C155-GAL4, UAS-mCD8-GFP, hsf1p;; FRT2A, tub-Gal80 (Liquan Luo), w, UAS-mCD8-GFP, hsf1p;; FRT82B, tubGAL4, tub-Gal80 (Laura Buttitta).

Clonal analysis

To generate MARCM clones, virgin females from MARCM-ready lines described above were crossed to control males and experimental males except for MARCM19A wherein virgin females from FRT19A, *e(y)1/Tafy¹⁹⁰* or *Trf2^{G0071}* were crossed to males from the MARCM-ready line for FRT19A. F1 larvae at 24 h after larval hatching (ALH) were heat-shocked for 1 h at 37°C, allowed to recover for 24 h at 18°C and further aged for 72 h at 25°C before dissection.

Immunofluorescence and confocal microscopy

The following antibodies were used: rabbit anti-GFP (1:500, Life Technologies A11122), chicken anti-GFP (1:250, Aves Labs GFP-1010), rabbit anti-DsRed (1:250, Clontech, 632496), mouse anti-HA (1:500, abcam 130275), mouse anti-FLAG (1:250, Sigma-Aldrich F3165), guinea pig anti-Deadpan (1:1000, James Skeath, Washington University), rat anti-Deadpan (abcam 195172), rabbit anti-Asense [1:500, Yuh Nung Jan, UCSF (Brand et al., 1993)], rabbit anti-Bazooka [1:500, (Ohshiro et al., 2000)] Fumio Matsuzaki, RIKEN Center for Developmental Biology, rabbit anti-Inscuteable [1:250, Fengwei Yu, TEMASEK Life Sciences Laboratory (Kraut and Campos-Ortega, 1996)], mouse anti-Prospero (1:50, MR1A from DSHB), rat anti-Elav (1:100, 7E8A10 from DSHB), rabbit anti-aPKC ζ (1:500, Santa Cruz sc-216, discontinued), rabbit anti-Cyclin E (1:250, Santa Cruz sc-33748, discontinued), mouse anti-phospho-Histone H3 (1:1000, Cell Signaling 9706), rabbit anti-phospho Histone H3 (1:1000, Millipore 05-817), mouse anti-TAF4 [1:100, 3E12 clone, Robert Tjian, UC Berkeley (Marr et al., 2006)], rabbit anti-TBP [1:500, James Kadonaga, UCSD (Wang et al., 2014)]. Larval brains were dissected in either PBS or Schneider's *Drosophila* media (21720-024, Thermo Fisher Scientific), fixed in 4% paraformaldehyde (Electron Microscopy Sciences) in PBS-T (PBS with 0.5% Triton X-100) for 20 min. After fixation, brains were washed in PBS-T for 10 min three times and blocked in PBS-T with 5% normal goat serum (005-000-121 Jackson ImmunoResearch Laboratories) and 1% BSA (A30075-250.0, Research Products International) for 1 h. Fixed brains were incubated with the relevant primary antibody solutions at the dilutions shown above for either 3 h at RT or overnight at 4°. The following day, brains were rinsed and washed for 10 min three times and then incubated in secondary antibody solution for 2 h at room temperature. After incubation with Alexa Fluor secondary antibodies (1:400; Thermo Fisher Scientific), three 10 min washes were performed and brains were mounted in Vectashield (Vector Laboratories; H-1200). Images were acquired on a Zeiss LSM780, processed with Fiji and figures were assembled with Inkscape 0.92.2. For NSC quantification, z-stacks of brain lobes were acquired with a step size of 2 μ m and central brain NSCs (large Dpn⁺ cells) were counted manually using the Cell Counter plugin in Fiji (Schindelin et al., 2012). For EdU labeling, dissected brains were incubated in 100 μ g/ μ l in Schneider's medium at 25° for 2 h with rocking. After fixation and antibody staining, EdU incorporation was detected following the manufacturer's protocol (Thermo Fisher Scientific, C10339).

NSCs sorting and RNA sequencing

Wandering third instar larvae from control or experimental genotypes were collected and washed once in phosphate-buffered saline (PBS), dissected in supplemented Schneider's medium [10% fetal bovine serum, 2% Pen/Strep (15140122, Thermo Fisher Scientific), 20 mM L-Glutamine (G7513, Sigma-Aldrich), L-Glutathione (G6013, Sigma-Aldrich) 5 mg/ml, Insulin (I0516, Sigma-Aldrich) 20 mg/ml, 20-Hydroxy-Ecdysone (H5142, Sigma-Aldrich) 1 mg/ml] and brains were collected and washed in cold Rinaldini solution. Next, they were enzymatically dissociated in Rinaldini solution with 1 mg/ml collagenase I (C0130, Sigma-Aldrich) and 1 mg/ml of papain (P4762, Sigma-Aldrich) for 1 h at 30°C. Brains were washed twice with Rinaldini solution and twice more with supplemented Schneider's medium. Brains were manually disrupted with a pipette tip in 200 μ l supplemented Schneider's medium. After filtering the cell suspension using a Flowmi tip strainer (H13680-0040, Bel-Art SP Scienceware), NSCs from control or

experimental genotypes were sorted in triplicate from brains expressing mCherry, TBP, TRF2, TAF5 or TAF9 RNAi transgenes on a BD Aria 2 essentially according to (Harzer et al., 2013), except that we used a 100 μ m nozzle and added DAPI (D9542, Sigma-Aldrich) at 1 μ g/ μ l to exclude dead cells. We obtained 10,000–15,000 putative NSCs from each sort. Sorted NSCs in TRIzol were homogenized with a pestle and then RNA was extracted according to the manufacturer's instructions, using Glycoblue 500 μ g/ μ l (AM9516, Ambion) as a co-precipitant. RNA was then eluted in 15 μ l of RNase-free water. Next, we used SMART-seq v4 ultra-low input kit (634889, Clontech) to generate double-stranded cDNA for each replicate, using 1 ng of total RNA as input. 1 ng of the resulting cDNA, amplified with 11 cycles of PCR in the cDNA amplification step, was used to prepare sequencing libraries with the Nextera XT kit (Illumina). Paired-end sequencing (50 bp) was performed on an Illumina HiSeq 2500 and the quality control matrix was generated for all samples using RNA-SeQC (DeLuca et al., 2012). RNA-seq reads were aligned to the *Drosophila melanogaster* dm6 genome using TopHat v2.1.0 (Trapnell et al., 2009) Gene counts were generated using the Python package HTSeq v0.6.0 (Anders et al., 2015) with the 'intersection-strict' overlap mode. Differentially expressed genes, defined as $|\log_2(\text{ratio})| \geq 1$ with the FDR set at 5%, were identified using the Bioconductor package edgeR, v3.16.5 (Robinson et al., 2010) after removing lowly expressed genes. The quality control steps described above prompted us to exclude the TAF5 samples. Over-represented GO terms for genes that were either significantly up or downregulated were identified using the Bioconductor package goseq, v1.26.0. RNA-seq data has been deposited with the Gene Expression Omnibus under series GSE120433, subseries GSE120430.

Targeted DamID (TaDa)

To generate TaDa transgenes, cDNAs for TBP (LD44083), TRF2S (LD27895) and TAF5 (LD42828) were cloned in frame into pUASTattB-LT3-NDam plasmid (kindly provided by Andrea Brand, Gurdon Institute) with ϕ C3-mediated site-specific integration at the attP2 site on chromosome III (strain genotype y w67c23; P {CaryPatt2}). Transformants were generated by BestGene Inc (Chino Hills, USA). The UAS-Dam, UAS-Dam-TBP, UAS-Dam-TRF2S and UAS-Dam-TAF5 transgenes were induced for 72 h at 30° using a wormiuGAL4, UAS-GFP, tubGAL80^{ts} driver. Genomic DNA from 100 nervous systems each was extracted in duplicate, processed and amplified essentially as described in (Marshall et al., 2016), except that removal of DamID adaptors was performed before DNA shearing on a Covaris S2. Library preparation and 50 bp single end sequencing was performed on a HiSeq2500 by the Fred Hutch genomics shared resource. Sequencing data was processed via damidseq_pipeline (Marshall and Brand, 2015) (https://owenjm.github.io/damidseq_pipeline/). This pipeline includes steps of sequence alignment, read extension, binned counts, normalization, pseudocount addition and final ratio file generation. Raw reads were mapped to the *Drosophila melanogaster* genome (ftp://ftp.flybase.net/genomes/Drosophila_melanogaster/dmel_r6.14_FB2017_01, version dmel_r6.14_FB2017_01). The find peaks software (https://github.com/owenjm/find_peaks) was used to call significant peaks present in the dataset. The output log₂ ratio files was converted to TDF for viewing in IGV using igvtools. The annotation and further analysis of significant peaks were done using HOMER (<http://homer.ucsd.edu/homer/index.html>, version v4.9). Principal Component Analysis and Spearman correlation coefficients of the read counts showed high correlation between the two sequencing runs (Fig. S6A,B), but because there was some variability between peaks that were called, and we wanted to identify genes co-bound either by TBP and TAF5 or between TRF2S and TAF5, we used a less stringent FDR of 0.05 and considered peaks identified in either replicate. The DamID-seq data has been deposited with the Gene Expression Omnibus under series GSE120433, subseries GSE120432.

Acknowledgements

We thank Spyros Artavanis-Tsakonas, Andrea Brand, Laura Buttitta, Shelagh Campbell, Wu-Min Deng, Chris Doe, Jean-Michel Gibert, Catarina Homem, Yuh Nung Jan, James Kadonaga, Qinghua Liu, Liquan Luo, Fumio Matsuzaki, James Skeath, Robert Tjian and Fengwei Yu for providing flies and/or antibodies, the Developmental Studies Hybridoma Bank (DSHB) for antibodies, the Bloomington Stock Center (NIH P40OD018537), TRIP at Harvard Medical School (NIH/NIGMS

R01-GM084947) and the Kyoto Stock Center and Vienna Drosophila Resource Center (VDRC) for providing fly stocks for this study. We are also indebted to the imaging, flow cytometry and genomics shared resources staff at Fred Hutch, in particular to Ms Qing Zhang.

Competing interests

R.N.E is on the scientific advisory boards of Kronos Bio and Shenogen Pharma, but there is absolutely no overlap/conflict with the present work.

Author contributions

Conceptualization: A.N., R.N.E.; Validation: A.N., R.N.E.; Formal analysis: A.N., R.N.E.; Investigation: A.N.; Resources: A.N.; Writing - original draft: A.N.; Writing - review & editing: A.N., R.N.E.; Visualization: A.N.; Supervision: R.N.E.; Project administration: R.N.E.; Funding acquisition: A.N., R.N.E.

Funding

A.N. was a fellow of the Jane Coffin Childs Memorial Fund for Medical Research and a Trainee of the Chromosome Metabolism and Cancer Training Grant (2T32CA009657). This work was also funded by grants CA057138 and NS090037 from the National Institutes of Health to R.N.E. The funders had no role in study design, data collection and analysis, decision to publish, or preparation of the manuscript.

Data availability

'Identification of transcriptional targets of a network of *Drosophila* core promoter factors in neural stem cells' available under accession number GSE120430.
'Identification of genomic binding sites of a network of core promoter factors in developing *Drosophila* brains' available under accession number GSE120432.
'A network of core promoter factors in developing *Drosophila* brains' available under accession number GSE120433.

Supplementary information

Supplementary information available online at <http://bio.biologists.org/lookup/doi/10.1242/bio.042168.supplemental>

References

- Anders, S., Pyl, P. T. and Huber, W. (2015). HTSeq—a Python framework to work with high-throughput sequencing data. *Bioinformatics* **31**, 166–169.
- Andersen, P. R., Tirian, L., Vunjak, M. and Brennecke, J. (2017). A heterochromatin-dependent transcription machinery drives piRNA expression. *Nature* **549**, 54–59.
- Aneichyk, T., Hendriks, W. T., Yadav, R., Shin, D., Gao, D., Vaine, C. A., Collins, R. L., Domingo, A., Currall, B., Stortchevoi, A. et al. (2018). Dissecting the causal mechanism of X-linked dystonia-Parkinsonism by integrating genome and transcriptome assembly. *Cell* **172**, 897–909.e21.
- Bello, B. C., Izergina, N., Caussinus, E. and Reichert, H. (2008). Amplification of neural stem cell proliferation by intermediate progenitor cells in *Drosophila* brain development. *Neural Dev.* **3**, 5.
- Berger, C., Harzer, H., Burkard, T. R., Steinmann, J., van der Horst, S., Laurenson, A.-S., Novatchkova, M., Reichert, H. and Knoblich, J. A. (2012). FACS purification and transcriptome analysis of *Drosophila* neural stem cells reveals a role for Klumpfuss in self-renewal. *Cell Rep.* **2**, 407–418.
- Boone, J. Q. and Doe, C. Q. (2008). Identification of *Drosophila* type II neuroblast lineages containing transit amplifying ganglion mother cells. *Dev. Neurobiol.* **68**, 1185–1195.
- Bowman, S. K., Rolland, V., Betschinger, J., Kinsey, K. A., Emery, G. and Knoblich, J. A. (2008). The tumor suppressors Brat and Numb regulate transit-amplifying neuroblast lineages in *Drosophila*. *Dev. Cell* **14**, 535–546.
- Bragg, D. C., Mangalaphiban, K., Vaine, C. A., Kulkarni, N. J., Shin, D., Yadav, R., Dhakal, J., Ton, M.-L., Cheng, A., Russo, C. T. et al. (2017). Disease onset in X-linked dystonia-parkinsonism correlates with expansion of a hexameric repeat within an SVA retrotransposon in TAF1. *Proc. Natl. Acad. Sci. USA* **114**, E11020–E11028.
- Brand, M., Jarman, A. P., Jan, L. Y. and Jan, Y. N. (1993). *asense* is a *Drosophila* neural precursor gene and is capable of initiating sense organ formation. *Development* **119**, 1–17.
- Chell, J. M. and Brand, A. H. (2010). Nutrition-responsive glia control exit of neural stem cells from quiescence. *Cell* **143**, 1161–1173.
- Chen, Z. and Manley, J. L. (2000). Robust mRNA transcription in chicken DT40 cells depleted of TAF(II)31 suggests both functional degeneracy and evolutionary divergence. *Mol. Cell. Biol.* **20**, 5064–5076.
- Choksi, S. P., Southall, T. D., Bossing, T., Edoff, K., DE Wit, E., Fischer, B. E., VAN Steensel, B., Micklem, G. and Brand, A. H. (2006). Prospero acts as a binary switch between self-renewal and differentiation in *Drosophila* neural stem cells. *Dev. Cell* **11**, 775–789.
- Coronado, D., Godet, M., Bourillot, P.-Y., Taponnier, Y., Bernat, A., Petit, M., Afanassieff, M., Markossian, S., Malashicheva, A., Iacone, R. et al. (2013). A short G1 phase is an intrinsic determinant of naïve embryonic stem cell pluripotency. *Stem Cell Res.* **10**, 118–131.
- Davie, K., Janssens, J., Koldere, D., DE Waegeneer, M., Pech, U., Kreft, L., Aibar, S., Makhzami, S., Christiaens, V., Bravo Gonzalez-Blas, C. et al. (2018). A single-cell transcriptome atlas of the aging *Drosophila* brain. *Cell* **174**, 982–998.
- Deluca, D. S., Levin, J. Z., Sivachenko, A., Fennell, T., Nazaire, M.-D., Williams, C., Reich, M., Winckler, W. and Getz, G. (2012). RNA-SeQC: RNA-seq metrics for quality control and process optimization. *Bioinformatics* **28**, 1530–1532.
- Dietzl, G., Chen, D., Schnorrer, F., Su, K.-C., Barinova, Y., Fellner, M., Gasser, B., Kinsey, K., Oettel, S., Scheiblaue, S. et al. (2007). A genome-wide transgenic RNAi library for conditional gene inactivation in *Drosophila*. *Nature* **448**, 151–156.
- Duttke, S. H. C., Doolittle, R. F., Wang, Y.-L. and Kadonaga, J. T. (2014). TRF2 and the evolution of the bilateria. *Genes Dev.* **28**, 2071–2076.
- El-Saafin, F., Curry, C., Ye, T., Garnier, J.-M., Kolb-Cheyne, I., Stierle, M., Downer, N. L., Dixon, M. P., Negroni, L., Berger, I. et al. (2018). Homozygous TAF8 mutation in a patient with intellectual disability results in undetectable TAF8 protein, but preserved RNA Polymerase II transcription. *Hum. Mol. Genet.* **27**, 2171–2186.
- Fan, W., Lam, S. M., Xin, J., Yang, X., Liu, Z., Liu, Y., Wang, Y., Shui, G. and Huang, X. (2017). *Drosophila* TRF2 and TAF9 regulate lipid droplet size and phospholipid fatty acid composition. *PLoS Genet.* **13**, e1006664.
- Fish, J. L., Kosodo, Y., Enard, W., Paabo, S. and Huttner, W. B. (2006). Aspm specifically maintains symmetric proliferative divisions of neuroepithelial cells. *Proc. Natl. Acad. Sci. USA* **103**, 10438–10443.
- Gibert, J.-M. and Karch, F. (2011). The Polycomb group protein CRAMPED is involved with TRF2 in the activation of the histone H1 gene. *Chromosoma* **120**, 297–307.
- Goodrich, J. A. and Tjian, R. (2010). Unexpected roles for core promoter recognition factors in cell-type-specific transcription and gene regulation. *Nat. Rev. Genet.* **11**, 549–558.
- Harzer, H., Berger, C., Conder, R., Schmauss, G. and Knoblich, J. A. (2013). FACS purification of *Drosophila* larval neuroblasts for next-generation sequencing. *Nat. Protoc.* **8**, 1088–1099.
- Hellman-Aharony, S., Smirin-Yosef, P., Halevy, A., Pasmanik-Chor, M., Yeheskel, A., Har-Zahav, A., Maya, I., Straussberg, R., Dahary, D., Haviv, A. et al. (2013). Microcephaly thin corpus callosum intellectual disability syndrome caused by mutated TAF2. *Pediatr. Neurol.* **49**, 411–416.e1.
- Herrera, F. J., Yamaguchi, T., Roelink, H. and Tjian, R. (2014). Core promoter factor TAF9B regulates neuronal gene expression. *eLife* **3**, e02559.
- Hiller, M., Chen, X., Pringle, M. J., Suchorski, M., Sancak, Y., Viswanathan, S., Bolival, B., Lin, T.-Y., Marino, S. and Fuller, M. T. (2004). Testis-specific TAF homologs collaborate to control a tissue-specific transcription program. *Development* **131**, 5297–5308.
- Hochheimer, A., Zhou, S., Zheng, S., Holmes, M. C. and Tjian, R. (2002). TRF2 associates with DREF and directs promoter-selective gene expression in *Drosophila*. *Nature* **420**, 439–445.
- Homem, C. C. F. and Knoblich, J. A. (2012). *Drosophila* neuroblasts: a model for stem cell biology. *Development* **139**, 4297–4310.
- Hsu, T.-C., Wang, C.-K., Yang, C.-Y., Lee, L.-C., Hsieh-Li, H.-M., Ro, L.-S., Chen, C.-M., Lee-Chen, G.-J. and Su, M.-T. (2014). Deactivation of TBP contributes to SCA17 pathogenesis. *Hum. Mol. Genet.* **23**, 6878–6893.
- Kedmi, A., Zehavi, Y., Glick, Y., Orenstein, Y., Ideses, D., Wachtel, C., Doniger, T., Waldman Ben-Asher, H., Muster, N., Thompson, J. et al. (2014). *Drosophila* TRF2 is a preferential core promoter regulator. *Genes Dev.* **28**, 2163–2174.
- Kraut, R. and Campos-Ortega, J. A. (1996). *inscuteable*, a neural precursor gene of *Drosophila*, encodes a candidate for a cytoskeleton adaptor protein. *Dev. Biol.* **174**, 65–81.
- Lai, S.-L., Miller, M. R., Robinson, K. J. and Doe, C. Q. (2012). The Snail family member *Worniu* is continuously required in neuroblasts to prevent Elav-induced premature differentiation. *Dev. Cell* **23**, 849–857.
- Lancaster, M. A., Renner, M., Martin, C.-A., Wenzel, D., Bicknell, L. S., Hurler, M. E., Homfray, T., Penninger, J. M., Jackson, A. P. and Knoblich, J. A. (2013). Cerebral organoids model human brain development and microcephaly. *Nature* **501**, 373–379.
- Lange, C. and Calegari, F. (2010). Cdks and cyclins link G1 length and differentiation of embryonic, neural and hematopoietic stem cells. *Cell Cycle* **9**, 1893–1900.
- Langer, D., Martianov, I., Alpern, D., Rhinn, M., Keime, C., Dollé, P., Mengus, G. and Davidson, I. (2016). Essential role of the TFIIID subunit TAF4 in murine embryogenesis and embryonic stem cell differentiation. *Nat. Commun.* **7**, 11063.
- Lee, T. and Luo, L. (1999). Mosaic analysis with a repressible cell marker for studies of gene function in neuronal morphogenesis. *Neuron* **22**, 451–461.
- Lee, C.-Y., Robinson, K. J. and Doe, C. Q. (2006). Lgl, Pins and aPKC regulate neuroblast self-renewal versus differentiation. *Nature* **439**, 594–598.
- Lee, J. H., Lee, J. E., Kahng, J. Y., Kim, S. H., Park, J. S., Yoon, S. J., Um, J.-Y., Kim, W. K., Lee, J.-K., Park, J. et al. (2018). Human glioblastoma arises from subventricular zone cells with low-level driver mutations. *Nature* **560**, 243–247.

- Li, L., Anderson, S., Secombe, J. and Eisenman, R. N. (2013). The *Drosophila* ubiquitin-specific protease Puffeye regulates dMyc-mediated growth. *Development* **140**, 4776-4787.
- Liang, C., Wang, Y., Murota, Y., Liu, X., Smith, D., Siomi, M. C. and Liu, Q. (2015). TAF11 assembles the RISC loading complex to enhance RNAi efficiency. *Mol. Cell* **59**, 807-818.
- Marr, M. T., Il, Isogai, Y., Wright, K. J. and Tjian, R. (2006). Coactivator cross-talk specifies transcriptional output. *Genes Dev.* **20**, 1458-1469.
- Marshall, O. J. and Brand, A. H. (2015). damidseq_pipeline: an automated pipeline for processing DamID sequencing datasets. *Bioinformatics* **31**, 3371-3373.
- Marshall, O. J., Southall, T. D., Cheetham, S. W. and Brand, A. H. (2016). Cell-type-specific profiling of protein-DNA interactions without cell isolation using targeted DamID with next-generation sequencing. *Nat. Protoc.* **11**, 1586-1598.
- Maston, G. A., Zhu, L. J., Chamberlain, L., Lin, L., Fang, M. and Green, M. R. (2012). Non-canonical TAF complexes regulate active promoters in human embryonic stem cells. *eLife* **1**, e00068.
- Neumüller, R. A., Richter, C., Fischer, A., Novatchkova, M., Neumüller, K. G. and Knoblich, J. A. (2011). Genome-wide analysis of self-renewal in *Drosophila* neural stem cells by transgenic RNAi. *Cell Stem Cell* **8**, 580-593.
- Ohshiro, T., Yagami, T., Zhang, C. and Matsuzaki, F. (2000). Role of cortical tumour-suppressor proteins in asymmetric division of *Drosophila* neuroblast. *Nature* **408**, 593-596.
- O'rawe, J. A., Wu, Y., Dörfel, M. J., Rope, A. F., Au, P. Y. B., Parboosingh, J. S., Moon, S., Kousi, M., Kosma, K., Smith, C. S. et al. (2015). TAF1 variants are associated with dysmorphic features, intellectual disability, and neurological manifestations. *Am. J. Hum. Genet.* **97**, 922-932.
- Otsuki, L. and Brand, A. H. (2018). Cell cycle heterogeneity directs the timing of neural stem cell activation from quiescence. *Science* **360**, 99-102.
- Pijnappel, W. W., Esch, D., Baltissen, M. P., Wu, G., Mischerikow, N., Bergsma, A. J., van der Wal, E., Han, D. W., Bruch, H., Moritz, S. et al. (2013). A central role for TFIID in the pluripotent transcription circuitry. *Nature* **495**, 516-519.
- Price, D. M., Jin, Z., Rabinovitch, S. and Campbell, S. D. (2002). Ectopic expression of the *Drosophila* Cdk1 inhibitory kinases, *Wee1* and *Myt1*, interferes with the second mitotic wave and disrupts pattern formation during eye development. *Genetics* **161**, 721-731.
- Robinson, M. D., McCarthy, D. J. and Smyth, G. K. (2010). edgeR: a Bioconductor package for differential expression analysis of digital gene expression data. *Bioinformatics* **26**, 139-140.
- Rooms, L., Reyniers, E., Scheers, S., VAN Luijk, R., Wauters, J., VAN Aerschot, L., Callaerts-Vegh, Z., D'hooge, R., Mengus, G., Davidson, I. et al. (2006). TBP as a candidate gene for mental retardation in patients with subtelomeric 6q deletions. *Eur. J. Hum. Genet.* **14**, 1090-1096.
- Rust, K., Tiwari, M. D., Mishra, V. K., Grawe, F. and Wodarz, A. (2018). Myc and the Tip60 chromatin remodeling complex control neuroblast maintenance and polarity in *Drosophila*. *EMBO J.* **37**, e98659.
- Schertel, C., Huang, D., Björklund, M., Bischof, J., Yin, D., Li, R., Wu, Y., Zeng, R., Wu, J., Taipale, J. et al. (2013). Systematic screening of a *Drosophila* ORF library in vivo uncovers Wnt/Wg pathway components. *Dev. Cell* **25**, 207-219.
- Schindelin, J., Arganda-Carreras, I., Frise, E., Kaynig, V., Longair, M., Pietzsch, T., Preibisch, S., Rueden, C., Saalfeld, S., Schmid, B. et al. (2012). Fiji: an open-source platform for biological-image analysis. *Nat. Methods* **9**, 676-682.
- Schuldiner, O., Berndik, D., Levy, J. M., Wu, J. S., Luginbuhl, D., Gontang, A. C. and Luo, L. (2008). piggyBac-based mosaic screen identifies a postmitotic function for cohesin in regulating developmental axon pruning. *Dev. Cell* **14**, 227-238.
- Şentürk, M. and Bellen, H. J. (2017). Genetic strategies to tackle neurological diseases in fruit flies. *Curr. Opin. Neurobiol.* **50**, 24-32.
- Siegrist, S. E., Haque, N. S., Chen, C.-H., Hay, B. A. and Hariharan, I. K. (2010). Inactivation of both Foxo and reaper promotes long-term adult neurogenesis in *Drosophila*. *Curr. Biol.* **20**, 643-648.
- Southall, T. D., Gold, K. S., Egger, B., Davidson, C. M., Caygill, E. E., Marshall, O. J. and Brand, A. H. (2013). Cell-type-specific profiling of gene expression and chromatin binding without cell isolation: assaying RNA Pol II occupancy in neural stem cells. *Dev. Cell* **26**, 101-112.
- Takada, S., Lis, J. T., Zhou, S. and Tjian, R. (2000). A TRF1:BRF complex directs *Drosophila* RNA polymerase III transcription. *Cell* **101**, 459-469.
- Tawamie, H., Martianov, I., Wohlfahrt, N., Buchert, R., Mengus, G., Uebe, S., Janiri, L., Hirsch, F. W., Schumacher, J., Ferrazzi, F. et al. (2017). Hypomorphic pathogenic variants in TAF13 are associated with autosomal-recessive intellectual disability and microcephaly. *Am. J. Hum. Genet.* **100**, 555-561.
- Thacker, S. A., Bonnette, P. C. and Duronio, R. J. (2003). The contribution of E2F-regulated transcription to *Drosophila* PCNA gene function. *Curr. Biol.* **13**, 53-58.
- Trapnell, C., Pachter, L. and Salzberg, S. L. (2009). TopHat: discovering splice junctions with RNA-Seq. *Bioinformatics* **25**, 1105-1111.
- Verheyen, E. M., Purcell, K. J., Fortini, M. E. and Artavanis-Tsakonas, S. (1996). Analysis of dominant enhancers and suppressors of activated Notch in *Drosophila*. *Genetics* **144**, 1127-1141.
- Wang, Y.-L., Duttke, S. H. C., Chen, K., Johnston, J., Kassavetis, G. A., Zeitlinger, J. and Kadonaga, J. T. (2014). TRF2, but not Tbp, mediates the transcription of ribosomal protein genes. *Genes Dev.* **28**, 1550-1555.
- Xie, G., Yu, Z., Jia, D., Jiao, R. and Deng, W. M. (2014). E(y)1/TAF9 mediates the transcriptional output of Notch signaling in *Drosophila*. *J. Cell Sci.* **127**, 3830-3839.
- Yang, C.-P., Fu, C.-C., Sugino, K., Liu, Z., Ren, Q., Liu, L.-Y., Yao, X., Lee, L. P. and Lee, T. (2016). Transcriptomes of lineage-specific *Drosophila* neuroblasts profiled by genetic targeting and robotic sorting. *Development* **143**, 411-421.
- Yuan, B., Pehlivan, D., Karaca, E., Patel, N., Charnig, W.-L., Gambin, T., Gonzaga-Jauregui, C., Sutton, V. R., Yesil, G., Bozdogan, S. T. et al. (2015). Global transcriptional disturbances underlie Cornelia de Lange syndrome and related phenotypes. *J. Clin. Invest.* **125**, 636-651.
- Zhou, H., Grubisic, I., Zheng, K., He, Y., Wang, P. J., Kaplan, T. and Tjian, R. (2013). Taf7l cooperates with Trf2 to regulate spermiogenesis. *Proc. Natl. Acad. Sci. USA* **110**, 16886-16891.
- Zhu, S., Wildonger, J., Barshow, S., Younger, S., Huang, Y. and Lee, T. (2012). The bHLH repressor Deadpan regulates the self-renewal and specification of *Drosophila* larval neural stem cells independently of Notch. *PLoS ONE* **7**, e46724.
- Zielke, N., Korzelius, J., van Straaten, M., Bender, K., Schuhknecht, G. F. P., Dutta, D., Xiang, J. and Edgar, B. A. (2014). Fly-FUCCI: a versatile tool for studying cell proliferation in complex tissues. *Cell Rep.* **7**, 588-598.